Acta Cryst. (1973). A**29**, 372

The Dependence of the Intensities of Diffuse Peaks on Scattering Angle in Neutron Diffraction

BY M. YESSIK

Scientific Research Staff, Ford Motor Company, Dearborn, Michigan 48121, *U.S.A.*,

S. A. WERNER

Scientific Research Staff, Ford Motor Company, Dearborn, Michigan 48121, *U.S.A.*

and

Department of Nuclear Engineering, University of Michigan, Ann Arbor, Michigan 48104, *U.S.A.*

AND H. SATO

Scientific Research Staff, Ford Motor Company, Dearborn, Michigan 48121, *U.S.A.*

(*Received* 13 *October* 1972; *accepted* 19 *January* 1973)

The variation of the intensity of diffuse peaks with scattering angle, $2\theta_s$, in neutron diffraction is investigated analytically. It is found that the intensity of a diffuse peak relative to a Bragg peak for a polycrystalline sample is much larger than for a single crystal. However, the diffuse intensity drops off much more rapidly with $2\theta_s$ in the polycrystalline case than in the single-crystal case. If the resolution of the instrument is 'sharp' in comparison with the extent of the diffuse scattering in reciprocal space, it is found that there is almost no variation of the intensity from one Brillouin zone to the next in a single-crystal experiment. These results are applied to the interpretation of an experiment on a Cu–Mn alloy.

Introduction

The main purpose of this work is to investigate in detail the dependence of the observed intensity on the scattering angle, $2\theta_s$, for elastic diffuse peaks, such as those due to short-range atomic ordering. The variation of the intensity of elastic scattering with $2\theta_s$ in a two-crystal neutron-diffraction experiment is generally represented by a term known as the Lorentz factor.* This factor is well known for a few special cases, such as the measurement of the integrated intensity of a Bragg reflection, in which it takes on a particularly simple functional form. In general, however, the Lorentz factor is a complicated function, depending upon both the density of scattering power in reciprocal space and the instrumental resolution. We shall thus wish to calculate an expression for the observed intensity of a diffuse peak. We shall do this for both the single-crystal and polycrystal cases.

In order to put the diffuse scattering on an absolute scale, it is most convenient to obtain a normalization with the Bragg peaks. The way in which this should be done is quite different for experiments on single crystals and for polycrystals, and appears not to be generally appreciated. Thus expressions for the intensities of Bragg peaks for both these cases will also be derived.

All together we shall consider four different cases: (1) single-crystal diffuse peaks, (2) polycrystal diffuse peaks, (3) single-crystal Bragg peaks and (4) polycrystal Bragg peaks.

The experimental arrangement is shown in Fig. 1 and is assumed to be the same in all cases. Therefore, a direct comparison of the measured intensity in each case with that of any other case can be readily made. We shall show, among other things, that for case 1 the Lorentz factor, when the resolution is sharp, becomes

$$L_1' = 1 , \tag{1}$$

(that is, *there is no variation at all of the intensity with scattering angle*). For case 2, again for sharp resolution, we shall find

$$L_2' = \frac{1}{\sin^2 \theta_s} . \tag{2}$$

For case 3, for the integrated intensity, when the detector collimation is relaxed, the Lorentz factor is given by

$$L_3' = \frac{1}{\sin 2\theta_s} . \tag{3}$$

For case 4, again for the integrated intensity, but with no restrictions on the detector collimation, we shall find

$$L_4 = \frac{1}{\sin \theta_s \sin 2\theta_s} . \tag{4}$$

These results for cases 3 and 4 are well known expressions for the Lorentz factor (*International Tables for X-ray Crystallography*, 1959).

* We are not concerned here with the possible variation of intensity with scattering angle due to a form factor or a temperature factor, both of which are assumed part of the structure factor.

As an example of the application of the results obtained here, an investigation of the diffuse peaks due to short-range order in Cu–25 at.% Mn will be discussed. It will be shown how the knowledge of the Lorentz factor for a single-crystal diffuse peak allowed the separation of nuclear and magnetic contributions to the diffuse peak.

While our main purpose in this paper is to discuss the Lorentz factor for aneutron-diffraction experiment, all of the results are directly applicable to X-ray diffraction simply by the inclusion of a polarization factor in the expressions for the intensities.

The resolution function

The intensity of elastic scattering in a two-crystal neutron-diffraction experiment is given by

$$I(\mathbf{Q}_0)=\varphi_0\int\left[\frac{\mathrm{d}\sigma}{\mathrm{d}\Omega}(\mathbf{Q})\right]_T R(\mathbf{Q}-\mathbf{Q}_0)\mathrm{d}^3\mathbf{Q} \qquad (5)$$

where $\mathbf{Q}_0$ is the most probable wave-vector change of the incident neutrons, $[\mathrm{d}\sigma/\mathrm{d}\Omega(\mathbf{Q})]_T$ is the total differential cross section of the sample for elastic scattering, $R(\mathbf{Q}-\mathbf{Q}_0)$ is the resolution function and φ_0 is the neutron flux incident on the monochromator per unit volume in $\mathbf{Q}$ space. The resolution function represents the probability of the detection of neutrons as a function of $\Delta\mathbf{Q}=\mathbf{Q}-\mathbf{Q}_0$ when the diffractometer is set to measure a scattering process corresponding to $\mathbf{Q}_0$. The form of the resolution function has been given by Cooper & Nathans (1968*a*) when the mosaic distribution of the monochromator and the transmission functions of the collimators are assumed to be Gaussian; namely

$$R(\mathbf{Q}-\mathbf{Q}_0)=R_0\exp\left\{-\tfrac{1}{2}\sum_{k=1}^{3}\sum_{l=1}^{3}M_{kl}\Delta_k Q\Delta Q_l\right\} \qquad (6)$$

where $\Delta Q_{1,2,3}=\Delta Q_{x,y,z}$. The axes x, y, and z are defined such that ΔQ_x is directed along $\mathbf{Q}_0$ and ΔQ_z is vertical. The general expressions for the M_{kl} are given by Cooper & Nathans (1968*a*). In this paper we shall assume that the in-pile collimation is relaxed. This is not a serious limitation and all of the results presented here can readily be extended to the more general case. The resulting expressions for the coefficients M_{kl} and R_0 are given in Appendix *A*.

All the points for which the resolution function has a particular value, *i.e.* the loci of constant probability of neutron detection, form an ellipsoid in reciprocal space and any path through the ellipsoid is a Gaussian. The particular ellipsoid for which $R(\mathbf{Q}-\mathbf{Q}_0)=R_0/2$ is called the resolution ellipsoid and is used to characterize the resolution function. Using the values of the instrumental parameters given in Table 1, the horizontal section of the resolution ellipsoid has been calculated for three different settings of the diffractometer as is shown by the solid lines in Fig. 2. It can be seen that the resolution ellipsoid becomes larger with increasing scattering vector. In other words neutrons scattered such that ΔQ is large have a higher probability of detection as $\mathbf{Q}_0$ becomes larger.

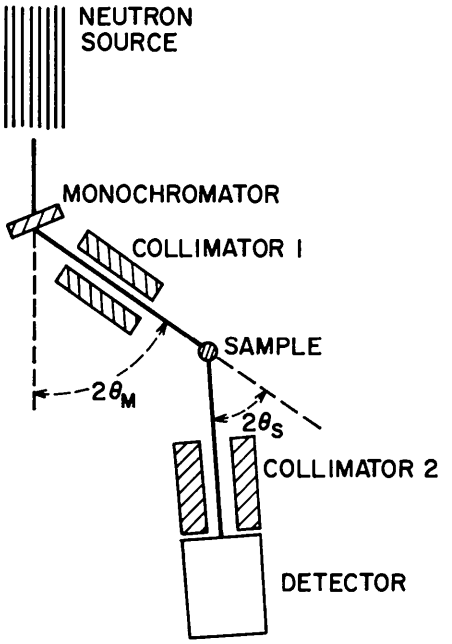

Fig. 1. Schematic experimental arrangement for a two-crystal neutron spectrometer.

Table 1. *Definitions and experimental values of the resolution parameters*

Name	Definition	Experimental value (°)	(rad)
α_1	Collimator 1 horizontal angle	0·18	0·0032
β_1	Collimator 1 vertical angle	0·33	0·0058
α_2	Collimator 2 horizontal angle	0·28	0·0049
β_2	Collimator 2 vertical angle	0·56	0·0098
η_M	Mosaic spread of monochromator	0·085	0·0015
η_{sh}	Horizontal mosaic spread of sample	0·25	0·0044
η_{sv}	Vertical mosaic spread of sample	0·25	0·0044
θ_M	Monochromator scattering angle	17·5	0·306
θ_s	Sample scattering angle	variable	
a	$\cos\theta_s$	variable	
b	$\sin\theta_s$	variable	
k_I	Most probable incident wave vector	5·83 Å^{-1}	
P_0	Maximum reflectivity of monochromator	—	
P_1	Maximum transmission of collimator 1	—	
P_2	Maximum transmission of collimator 2	—	
a_0	Lattice constant of sample	3·70 Å	

Note: The characteristic angles defined above are chosen such that the corresponding transmission functions equal $\exp(-\frac{1}{2})$ times their maximum values.

Equation (5) can be rewritten in a different form by noting that $[\mathrm{d}\sigma/\mathrm{d}\Omega(\mathbf{Q})]_T$ is the cross section integrated over the distribution of reciprocal-lattice vectors in the whole sample, *i.e.*

$$\left[\frac{\mathrm{d}\sigma}{\mathrm{d}\Omega}(\mathbf{Q})\right]_T=\int\frac{\mathrm{d}\sigma}{\mathrm{d}\Omega}(\mathbf{Q}-\mathbf{K})n(\mathbf{K})\mathrm{d}^3K \qquad (7)$$

where $d\sigma/d\Omega(\mathbf{Q}-\mathbf{K})$ is the scattering cross section for a single grain (or mosaic block), $n(\mathbf{K})$ describes the orientational distribution of grains in the sample and is normalized such that $\int n(\mathbf{K})d^3K = n_0$, the total number of grains in the sample. Equation (5) can then be written

$$I(\mathbf{Q}_0) = \varphi_0 \int\int \frac{d\sigma}{d\Omega}(\mathbf{Q}-\mathbf{K}) n(\mathbf{K}) R(\mathbf{Q}-\mathbf{Q}_0) d^3K d^3Q\,, \quad (8)$$

which, by a simple transformation of variables, is equivalent to

$$I(\mathbf{Q}_0) = \varphi_0 \int \frac{d\sigma}{d\Omega}(\mathbf{Q}) R'(\mathbf{Q}-\mathbf{Q}_0) d^3Q \quad (9)$$

where

$$R'(\mathbf{Q}-\mathbf{Q}_0) = \int n(\mathbf{K}) R(\mathbf{Q}-\mathbf{Q}_0+\mathbf{K}) d^3K\,. \quad (10)$$

Equation (9) is the form that we shall use in calculating the intensities for each of the four cases discussed in the introduction.

We can now write down explicitly the expression for $R'(\mathbf{Q}-\mathbf{Q}_0)$ for the two types of sample of interest here, *i.e.* a mosaic single crystal and a polycrystal. For the mosaic single crystal (whose expressions will be denoted by the subscript M), the orientational distribution of the mosaic blocks will be assumed to be Gaussian about some vector $\mathbf{K}_0$ and is given by

$$n_M(\mathbf{K}) = \frac{n_0 \delta(\Delta K_x)}{2\pi \eta_{sv}\eta_{sh} K_0^2} \times \exp\left\{-\tfrac{1}{2}\left[\left(\frac{\Delta K_y}{\eta_{sh}K_0}\right)^2 + \left(\frac{\Delta K_z}{\eta_{sv}K_0}\right)^2\right]\right\}, \quad (11)$$

where $\Delta\mathbf{K} = \mathbf{K} - \mathbf{K}_0$ and it is assumed that the mosaic spread is small, $\delta(\Delta K_x)$ is a delta function and the parameters are defined in Table 1. A vector diagram representing this situation is shown in Fig. 3(*a*). Assuming that the extent of the resolution function is small compared with Q_0 and performing the integration of equation (10) one obtains

$$R'_M(\mathbf{Q}-\mathbf{Q}_0) = R'_0 \exp\left\{-\tfrac{1}{2}\sum_{k,l=1}^{3} M'_{kl}\Delta Q_k \Delta Q_l\right\} \quad (12)$$

where

$$R'_0 = n_0 R_0 \cdot [(M_{33}K_0^2\eta_{sv}^2 + 1)(M_{22}K_0^2\eta_{sh}^2 + 1)]^{-1/2} \quad (13)$$

and

$$\begin{aligned} M'_{11} &= M_{11} - \frac{M_{12}^2 K_0^2 \eta_{sh}^2}{(M_{22}K_0^2\eta_{sh}^2 + 1)} \\ M'_{12} &= \frac{M_{12}}{(M_{22}K_0^2\eta_{sh}^2 + 1)} \\ M'_{22} &= \frac{M_{22}}{(M_{22}K_0^2\eta_{sh}^2 + 1)} \\ M'_{33} &= \frac{M_{33}}{(M_{33}K_0^2\eta_{sv}^2 + 1)}\,. \end{aligned} \quad (14)$$

We see that equation (12) has the same form as equation (6). This means that for a single-crystal sample the effective resolution function, *i.e.* the resolution function that includes the mosaic spread of the sample, can also be characterized by an ellipsoid in reciprocal space. This ellipsoid is given by $R'_M(\mathbf{Q}-\mathbf{Q}_0) = R'_0/2$. For the particular Cu–Mn single-crystal sample used in our experiment the single-crystal resolution ellipsoid is shown by the dashed lines in Fig. 2 for three settings of the diffractometer and can be directly compared with the original resolution ellipsoid. The effect on the resolution of the sample mosaic spread is to a first approximation simply to broaden the ellipsoid in the **y** and **z** directions. This is the expected result since the mosaic spread increases the extent of the total cross section only in the **y** and **z** directions, as can be seen from equations (7) and (11).

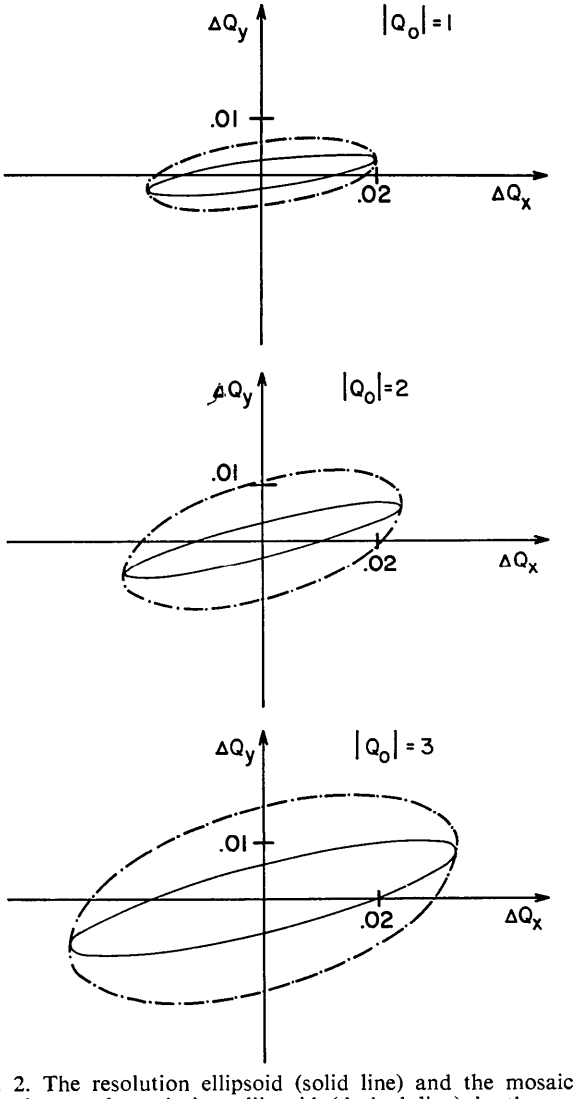

Fig. 2. The resolution ellipsoid (solid line) and the mosaic single-crystal resolution ellipsoid (dashed line) in the *xy* plane for three different values of $|Q_0| = 2|k_I| \sin\theta_s$. The values of $|Q_0|$ and $\Delta Q_{x,y}$ are in units of $(2\pi/a_0)$.

For a polycrystalline sample (denoted by the subscript P), the distribution function describing the orientation of the grains is independent of angle and is given by

$$n_P(\mathbf{K}) = \frac{n_0 \delta(\Delta K_x)}{4\pi K_0^2} \tag{15}$$

and the integration of equation (10) yields

$$R'_P(\mathbf{Q}-\mathbf{Q}_0) = \frac{n_0 R_0}{2K_0^2\sqrt{M_{22}M_{33}}} \times \exp\left\{-\tfrac{1}{2}\left(M_{11} - \frac{M_{12}^2}{M_{22}}\right)\Delta Q_x^2\right\}. \tag{16}$$

Thus the resolution function for a polycrystalline sample varies along only one direction in reciprocal space, namely, the direction parallel to $\mathbf{Q}_0$. A vector diagram for polycrystalline scattering is given in Fig. 3(*b*).

Thus we now have expressions for the resolution functions for both mono- and polycrystalline samples, and simply by specifying the form of the cross section in equation (9) we can determine the expressions for the intensities.

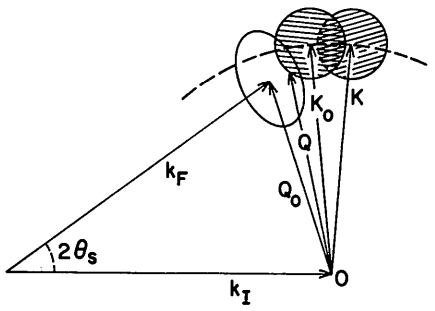

(*a*)

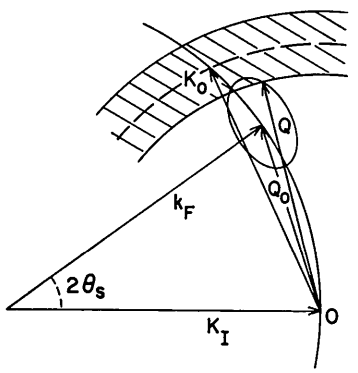

(*b*)

Fig. 3. (*a*) Schematic vector diagram in the horizontal plane of reciprocal space showing the scattering process for a mosaic single crystal. The shaded areas represent the scattering distributions from different mosaic grains and the open ellipse is the resolution ellipse. (*b*) Same as (*a*) for a polycrystal.

Diffuse scattering

For a diffuse peak the cross section can be written as

$$\frac{d\sigma}{d\Omega}(\mathbf{Q}) = A_0 f(\mathbf{Q}-\mathbf{K}_0) \tag{17}$$

where $f(\mathbf{Q}-\mathbf{K}_0)$ is the distribution of diffuse scattering power about some wave vector $\mathbf{K}_0$ in the grain at the center of the mosaic distribution and is normalized such that $\int f(\mathbf{Q}-\mathbf{K}_0)d^3Q = 1$. A_0 is given by

$$A_0 = (2\pi)^3 f_0 v_g |F|^2 / v_c^2, \tag{18}$$

where v_g is the average volume of a mosaic grain, v_c is the volume of a unit cell, F is the structure factor and f_0 is a constant factor dependent upon the degree of ordering. Although a diffuse peak may have many possible shapes, for the ensuing calculations we shall assume that the distribution of diffuse scattering is Gaussian. However, some of the results we shall obtain will be independent of the shape and all the results can be obtained for other shapes in an analogous manner.

If the diffuse peak is isotropic about $\mathbf{K}_0$ we can write

$$\frac{d\sigma}{d\Omega}(\mathbf{Q}-\mathbf{K}_0) = A_0(2\pi)^{-3/2}D^{-3} \times \exp\{-\tfrac{1}{2}(|\mathbf{Q}-\mathbf{K}_0|/D)^2\} \tag{19}$$

where D is the characteristic width of the diffuse peak in reciprocal space. In general the diffuse peak will not be isotropic and a simple anisotropic distribution to consider is an ellipsoidal peak. This choice fits our experimental data on Cu–Mn quite well.

The cross section can then be written

$$\frac{d\sigma}{d\Omega}(\mathbf{Q}-\mathbf{K}_0) = A_0(2\pi)^{-3/2}(D_{x'}D_{y'}D_{z'})^{-1} \times \exp\left\{-\tfrac{1}{2}\left[\left(\frac{\Delta\chi_{x'}}{D_{x'}}\right)^2 + \left(\frac{\Delta\chi_{y'}}{D_{y'}}\right)^2 + \left(\frac{\Delta\chi_{z'}}{D_{z'}}\right)^2\right]\right\} \tag{20}$$

where $\Delta\boldsymbol{\chi} = \mathbf{Q}-\mathbf{K}_0$ and $D_{x'}, D_{y'}, D_{z'}$ are the characteristic widths of the diffuse peak in the $\mathbf{x}', \mathbf{y}', \mathbf{z}'$ directions.

Case 1: *Diffuse scattering from a mosaic single crystal*

In order to calculate the observed intensity for the scattering cross section of equation (20), the single-crystal resolution function of equation (12) must be written in terms of coordinates coinciding with the symmetry of this cross section. After performing this coordinate transformation the intensity can be calculated from equation (9) and the result is

$$I_1(\Delta\mathbf{q}) = \frac{\varphi_0 A_0 (2\pi)^{-3/2}}{D_{x'}D_{y'}D_{z'}} C_0 \exp\left\{-\tfrac{1}{2}\sum_{k,l=1}^{3} C_{kl}\Delta q'_k \Delta q'_l\right\} \tag{21}$$

where $\Delta\mathbf{q} = \mathbf{Q}_0 - \mathbf{K}_0$ and $\Delta q'_{1,2,3} = \Delta q_{x',y',z'}$. The expressions for the coefficient C_0 and the matrix C_{kl} are given in Appendix *B*.

This result is the expression for the intensity of neutrons scattered from a single-crystal diffuse peak as a function of $\mathbf{Q}_0-\mathbf{K}_0$ where $\mathbf{Q}_0$ is the nominal setting of the diffractometer and $\mathbf{K}_0$ is the wave vector corresponding to the center of the diffuse-scattering cross section in the central mosaic grain. It can be seen from the expressions for the coefficients given in Appendix *B* that the measured intensity depends on the extent of the diffuse peak relative to the extent of the resolution function. If we consider the usual case where the extent of the resolution function in **Q** space is small compared with the diffuse peak, then the elements of the matrix C_{kl} reduce to

$$\begin{aligned} C'_{11}&=(D_{x'})^{-2}\\ C'_{22}&=(D_{y'})^{-2}\\ C'_{33}&=(D_{z'})^{-2}\\ C'_{12}&=0 \end{aligned} \tag{22}$$

and the coefficient C_0 reduces to

$$C'_0=(2\pi)^{3/2}R'_0[M'_{33}(M'_{22}M'_{11}-M'^2_{12})]^{-1/2}. \tag{23}$$

This means that the expression of equation (21) reduces to

$$I'_1(\mathbf{Q}_0-\mathbf{K}_0)=\varphi_0 C'_0\frac{\mathrm{d}\sigma}{\mathrm{d}\Omega}(\mathbf{Q}_0-\mathbf{K}_0)\,. \tag{24}$$

This same result can be arrived at in a conceptually simpler way directly from equation (9) which for this case is written as

$$I_1(\mathbf{Q}_0-\mathbf{K}_0)=\varphi_0\int\frac{\mathrm{d}\sigma}{\mathrm{d}\Omega}(\mathbf{Q}-\mathbf{K}_0)R'_M(\mathbf{Q}-\mathbf{Q}_0)\mathrm{d}^3Q\,. \tag{25}$$

The assumption that the extent of the resolution function is small compared with the diffuse peak is the same as the assumption that over the region of **Q** space where $R'_M(\mathbf{Q}-\mathbf{Q}_0)$ has appreciable values, $\mathrm{d}\sigma/\mathrm{d}\Omega(\mathbf{Q}-\mathbf{K}_0)$ is essentially constant. Therefore we can write equation (25) as

$$I'_1(\mathbf{Q}_0-\mathbf{K}_0)=\varphi_0\frac{\mathrm{d}\sigma}{\mathrm{d}\Omega}(\mathbf{Q}_0-\mathbf{K}_0)\int R'_M(\mathbf{Q}-\mathbf{Q}_0)\mathrm{d}^3Q \tag{26}$$

and performing the integration over the resolution function gives

$$I'_1(\mathbf{Q}_0-\mathbf{K}_0)=\varphi_0\frac{\mathrm{d}\sigma}{\mathrm{d}\Omega}(\mathbf{Q}_0-\mathbf{K}_0)\,(2\pi)^{3/2}R'_0$$

$$[M'_{33}(M'_{22}M'_{11}-M'^2_{12})]^{-1/2}=\varphi_0 C'_0\frac{\mathrm{d}\sigma}{\mathrm{d}\Omega}(\mathbf{Q}_0-\mathbf{K}_0) \tag{27}$$

which is the same result as that obtained in equation (24). The term C'_0, which is simply the integral of the single-crystal resolution function over all **Q** space, is, of course, independent of any coordinate transformation. By substituting the expressions for R'_o and M'_{kl} from equations (13) and (14) and using the relations given in Appendix *A* we have

$$C'_0=(2\pi)^{5/2}n_0P_0P_1P_2k_I^3\eta_M\alpha_1\beta_1\alpha_2\beta_2\ \mathrm{ctn}\ \theta_M\,. \tag{28}$$

The parameters are defined in Table 1. We can immediately see that C'_0 is independent of the scattering angle, $2\theta_s$. The interpretation of equation (27) is then that the intensity is directly proportional to the cross section of the diffuse peak at each point in **Q** space and there is no dependence of the intensity on scattering angle, *i.e.* the Lorentz factor, L'_1, is 1 as anticipated in equation (1). It can also be seen that in the derivation of equation (27) there is no assumption about the shape of the diffuse peak other than it be much larger than the resolution function, *i.e.* the shape could be Gaussian, Lorentzian, or anything else. Also we can see that C'_0 is independent of the mosaic spread of the sample.

Of course, as we have seen in Fig. 2 the resolution function broadens as **Q** increases or as $2\theta_s$ increases. Therefore, the assumption that the resolution function is small compared with the diffuse peak may only hold for small values of $2\theta_s$ even with fairly tight collimation. The intensity must then be calculated from the expression of equation (21). The peak intensity of the diffuse scattering is simply

$$I_1(\Delta\mathbf{q}=0)=\varphi_0 C_0\frac{\mathrm{d}\sigma}{\mathrm{d}\Omega}(\Delta\mathbf{q}=0) \tag{29}$$

and so the more general Lorentz factor for the peak is simply

$$L_1^0=C_0/C'_0\,. \tag{30}$$

As can be seen from the expression for C_0 given in Appendix *B* the value of L_1^0 depends upon the relative shapes of the resolution function and the diffuse peak. For a spherical diffuse peak the intensity falls off with $2\theta_s$ as shown in Fig. 4 for different values of the detector collimation constant α_2. However, since the resolution function rotates as well as broadens as $2\theta_s$ increases, for a nonspherical diffuse peak, the Lorentz factor depends upon the direction of **Q** as well as its magnitude. That is, the intensity varies differently for different directions of scans through the nonspherical diffuse peaks. An example is shown in Fig. 5 where L_1 is plotted for three different shapes of diffuse peaks

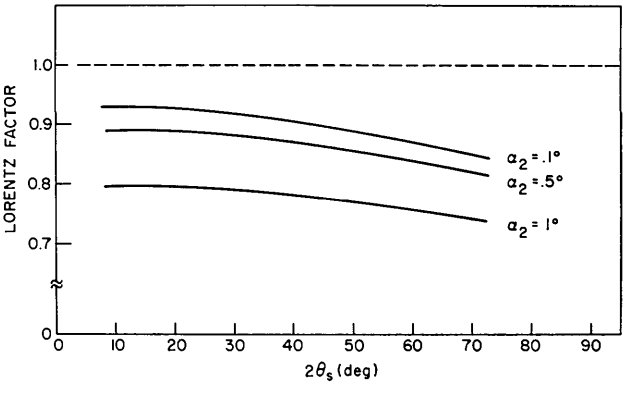

Fig. 4. The Lorentz factor L_1^0 for a spherical diffuse peak of size $D=0{\cdot}1\ (2\pi/a_0)$ for different values of α_2.

and for two different scans. In some cases it can be seen that the intensity actually increases with $2\theta_s$ for certain ranges of $2\theta_s$. In the examples the axes of the diffuse peaks are chosen parallel to the axes of the reciprocal lattice.

Case 2: Diffuse scattering from a polycrystal

From equations (16) and (9) the intensity is given by

$$I_2(\mathbf{Q}_0)=m_D\varphi_0\int\frac{\mathrm{d}\sigma}{\mathrm{d}\Omega}(\mathbf{Q})R_P'(\mathbf{Q}-\mathbf{Q}_0)\mathrm{d}^3Q \tag{31}$$

where m_D is the multiplicity for the diffuse peak. For simplicity let us use the isotropic cross section of equation (19). Then we have

$$I_2(Q_0)=\frac{m_D\varphi_0A_0}{(2\pi)^{3/2}D^3}\frac{n_0R_0}{2K_0^2(M_{22}M_{33})^{1/2}}\times\int\exp\left\{-\tfrac{1}{2}\left[(\Delta\chi_x^2+\Delta\chi_y^2+\Delta\chi_z^2)/D^2+\left(M_{11}-\frac{M_{12}^2}{M_{22}}\right)\Delta Q_x^2\right]\right\}\mathrm{d}^3Q \tag{32}$$

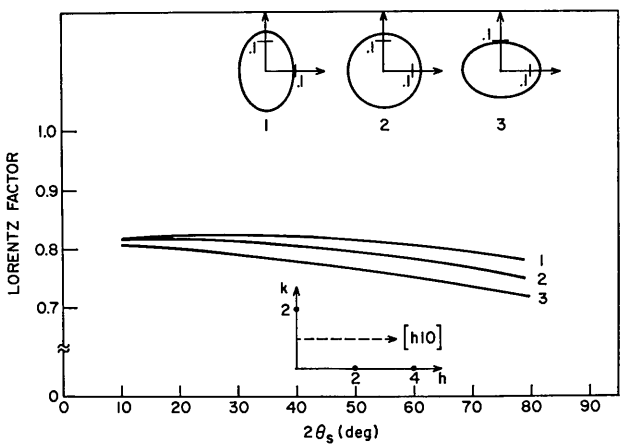

(a)

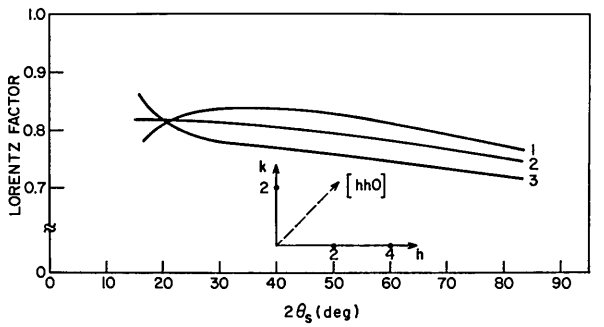

(b)

Fig. 5. (*a*) The Lorentz factor L_1^0 for a scan along [*h*10], and (*b*) L_1^0 for a scan along [*hh*0] both for three different shape diffuse peaks and for $\alpha_2=1°$. The diffuse peaks are dimensioned in units of $(2\pi/a_0)$.

where again $\Delta\chi=\mathbf{Q}-\mathbf{K}_0$. The integration can then be performed yielding

$$I_2(\Delta q_x)=\frac{m_D\varphi_0A_0}{2DK_0^2}\frac{n_0R_0}{\left\{\left[M_{33}M_{22}\left(M_{11}-\frac{M_{12}^2}{M_{22}}+\frac{1}{D^2}\right)\right]\right\}^{1/2}}\times\exp\left\{-\tfrac{1}{2}\left[\left(\frac{\Delta q_x}{D}\right)^2\left(1-\frac{1}{D^2}\frac{1}{\left(\frac{1}{D^2}+M_{11}-\frac{M_{12}^2}{M_{22}}\right)}\right)\right]\right\}. \tag{33}$$

where $\Delta q_x=|\mathbf{Q}_0-\mathbf{K}_0|_x$. Again, as in the single-crystal case, we see that the intensity depends on the extent of the diffuse peak relative to the resolution function. If the resolution ellipsoid is small compared with the diffuse peak the intensity is given by

$$I_2'(\Delta q_x)=\frac{m_D\varphi_0A_0}{(2\pi)^{3/2}2DK_0{}^2}C_0'\exp\{-\tfrac{1}{2}(\Delta q_x/D)^2\} \tag{34}$$

or

$$I_2'(\Delta q_x)=m_D\varphi_0\frac{D^2}{2K_0^2}C_0'\frac{\mathrm{d}\sigma}{\mathrm{d}\Omega}(\Delta q_x) \tag{35}$$

where

$$C_0'=\frac{n_0R_0(2\pi)^{3/2}}{\left[M_{33}M_{22}\left(M_{11}-\frac{M_{12}^2}{M_{22}}\right)\right]^{1/2}}. \tag{36}$$

This expression for C_0' is equivalent to that given by equation (23), and therefore independent of $2\theta_s$, since we have shown in equation (28) that C_0' is independent of the mosaic spread of the sample.

The intensity, $I_2'(\Delta q_x)$, is therefore directly proportional to the variation of the cross section in the **x** direction; however, there is a dependence on scattering angle due to the term $1/K_0{}^2$ and equation (35) can be rewritten as

$$I_2'(\Delta q_x)=m_D\varphi_0C_0'\frac{D^2}{8k_I{}^2}\frac{\mathrm{d}\sigma}{\mathrm{d}\Omega}(\Delta q_x)\frac{1}{\sin^2\theta_s}. \tag{37}$$

Therefore

$$L_2'=\frac{1}{\sin^2\theta_s} \tag{38}$$

as anticipated in equation (2).

Bragg scattering

In order to put the diffuse scattering on an absolute scale it is necessary to derive expressions for the Bragg reflections using the same mathematical formalism as in the previous section. For a Bragg reflection the cross section for elastic scattering is given by

$$\frac{\mathrm{d}\sigma}{\mathrm{d}\Omega}(\mathbf{Q})=B_0\delta(\mathbf{Q}-\mathbf{G}_0) \tag{39}$$

where $\mathbf{G}_0$ is a reciprocal lattice vector and $B_0=A_0/f_0$.

We are assuming that extinction is negligible. Equa-

tion (9) can now be written

$$I(\mathbf{Q}_0-\mathbf{G}_0)=\varphi_0 B_0\int\delta(\mathbf{Q}-\mathbf{G}_0)R'(\mathbf{Q}-\mathbf{Q}_0)\mathrm{d}^3Q$$
$$=\varphi_0 B_0 R'(\mathbf{Q}_0-\mathbf{G}_0)\,. \qquad (40)$$

Case 3: *Bragg scattering from a mosaic single crystal*

We can now write this result directly as

$$I_3(\mathbf{Q}_0-\mathbf{G}_0)=\varphi_0 B_0 R'_M(\mathbf{Q}_0-\mathbf{G}_0)\,. \qquad (41)$$

This is the intensity of a single-crystal Bragg reflection for a setting of the crystal and diffractometer corresponding to $\mathbf{Q}_0-\mathbf{G}_0\equiv\Delta\mathbf{q}$. Any scan in $\mathbf{Q}$ space along a linear path $\Delta\mathbf{q}$ is Gaussian and the variation in width of the Gaussian scans can be seen directly from the shape of the constant contours of the function $R'_M(\Delta\mathbf{q})$ as shown in Fig. 2.

If the crystal is rotated through the reflecting position, the integrated intensity can be readily obtained from equations (41) and (12) as

$$\mathscr{I}_3=\int I_3\mathrm{d}\omega=\varphi_0 B_0 R'_0\int\exp\{-\tfrac{1}{2}M'_{22}(\Delta q_y)^2\}\frac{\Delta q_y}{G_0} \qquad (42)$$

since $\Delta q_x=\Delta q_z=0$, and therefore

$$\mathscr{I}_3=\frac{\varphi_0 B_0 R'_0}{G_0}\left(\frac{2\pi}{M'_{22}}\right)^{1/2}. \qquad (43)$$

The term 'integrated intensity', however, is usually applied to the special case where the detector is sufficiently wide open to accept all of the Bragg scattered neutrons at each angular setting of the crystal. This is equivalent to the condition that α_2 and β_2 become large. In this case the expression of equation (43) simplifies to

$$\mathscr{I}'_3=C_3L'_3\,, \qquad (44)$$

where

$$C_3=\varphi_0 n_0 B_0 P_0 P_1 P_2(2\pi)^{3/2}\alpha_1\beta_1\eta_M\ \mathrm{ctn}\ \theta_M \qquad (45)$$

and

$$L'_3=\frac{1}{\sin 2\theta_s}\,. \qquad (46)$$

This expression, as expected, is independent of the mosaic spread of the sample. The Lorentz factor, L'_3, is the same as anticipated in equation (3).*

If now the more general expression for the integrated intensity, as given in equation (43), is written as $\mathscr{I}_3=C_3L_3$ then the more general Lorentz factor is given by

$$L_3=\frac{\dfrac{\varphi_0 B_0 R'_0}{G_0}\left(\dfrac{2\pi}{M'_{22}}\right)^{1/2}}{C_3}\,. \qquad (47)$$

This quantity is plotted as a function of $2\theta_s$ for various values of the detector collimation constant α_2 in Fig. 6(*a*). As can be seen L_3 varies most rapidly with $2\theta_s$ for tight collimation and gradually approaches the limiting value of $1/\sin 2\theta_s$ as the collimation is relaxed.

The intensity at the peak of the Bragg reflection ($\mathbf{Q}_0=\mathbf{G}_0$) from equation (41) is simply

$$I_3(\Delta\mathbf{q}=0)=\varphi_0 B_0 R'_0\,. \qquad (48)$$

As α_2 and β_2 become large this value approaches a limit given by

$$I'_3(\Delta\mathbf{q}=0)=(2\pi)^{-1/2}C_3\frac{1}{\sin 2\theta_s}$$
$$\times\left[\eta_{sh}^2+\left(\frac{\tan\theta_s}{\tan\theta_M}-1\right)^2\alpha_1^2+\frac{\tan^2\theta_s}{\tan^2\theta_M}\eta_M{}^2\right]^{-1/2}. \qquad (49)$$

Thus, in this limit, it is seen that the peak intensity varies as $1/\sin 2\theta_s$ modified by a term which is a function of the resolution parameters. We can write the general expression for the peak intensity from equation (48) as

$$I_3(\Delta\mathbf{q}=0)=(2\pi)^{-1/2}C_3L_3^0\,. \qquad (50)$$

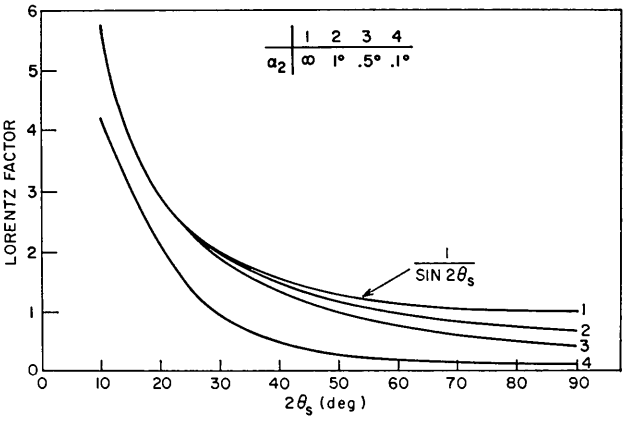

(*a*)

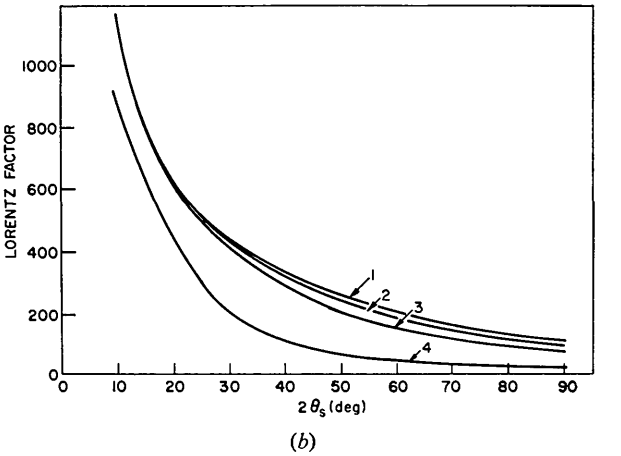

(*b*)

Fig. 6. (*a*) The Lorentz factor L_3, and (*b*) The Lorentz factor L_3^0 both as a function of $2\theta_s$ for four values of α_2 and with $\beta_2=\infty$.

* Equation (44) differs in form from the usual equation for integrated intensity which is written in terms of the neutron flux incident on the sample, I_0, instead of the neutron flux incident on the monochromator. In the present notation, $I_0=\varphi_0 k_I^3\alpha_1\beta_1\eta_M$ ctn θ_M so that the integrated intensity in terms of I_0 is written $\mathscr{I}'_3=I_0 n_0 B_0 P_2/k_I^3$ sin $2\theta_s$, a more familiar form.

The factor L_3^0 is shown in Fig. 6(*b*) for several values of α_2. As can be seen, L_3^0 varies most rapidly with $2\theta_s$ for tight detector collimation and approaches the limiting value of equation (49) as the collimation is relaxed.

Case 4: *Bragg scattering from a polycrystal*

From equations (40) and (16) this result can be written directly as

$$I_4(\Delta q_x)=m_B\varphi_0 n_0 B_0 R_P'(\Delta q_x)\,, \tag{51}$$

where m_B is the multiplicity of the Bragg reflection.

The intensity at the peak of the Bragg reflection is simply

$$I_4(\Delta q_x=0)=\frac{m_B\varphi_0 n_0 R_0}{2G_0^2(M_{22}M_{33})^{1/2}}\,. \tag{52}$$

When the horizontal aperture of the detector is wide enough to accept the entire width of the Debye–Scherrer ring, *i.e.* as α_2 becomes very large, then equation (52) simplifies to

$$I_4'(\Delta q_x=0)=C_4'L_4^{0\prime} \tag{53}$$

where

$$C_4'=\frac{m_B\beta_2}{4}(2\pi)^{-1/2}C_3 \tag{54}$$

and

$$L_4^{0\prime}=\frac{1}{\sin\theta_s\sin 2\theta_s}\,. \tag{55}$$

In the more general case of equation (52) we have

$$L_4^0=\frac{I_4(\Delta q_x=0)}{C_4'}=\frac{n_0B_0R_0}{2G_0^2(M_{22}M_{33})^{1/2}}\Big/C_4'\,. \tag{56}$$

This expression is plotted in Fig 7 for several values of α_2. It can be seen that L_4^0 varies most rapidly with $2\theta_s$ for tight collimation and gradually approaches the limiting value of $1/\sin\theta_s\sin 2\theta_s$ as α_2 increases.

The expression for the integrated polycrystalline intensity can be readily obtained from equations (51) and (16) as

$$\mathscr{I}_4=\int I_4(\Delta q_x)\mathrm{d}(2\theta_s)=\frac{m_B\varphi_0 n_0 B_0 R_0}{2G_0^2(M_{22}M_{33})^{1/2}} \times\int\exp\left\{-\tfrac{1}{2}\left(M_{11}-\frac{M_{12}^2}{M_{22}}\right)\Delta q_x^2\right\}\frac{\Delta q_x}{2k_I\cos\theta_s} \tag{57}$$

since $\Delta q_x=k_I\cos\theta_s\Delta(2\theta_s)$. Performing the integration yields

$$\mathscr{I}_4=C_4L_4 \tag{58}$$

where

$$C_4=(2\pi)^{1/2}\alpha_2C_4'$$

$$=\frac{m_B\alpha_2\beta_2}{4}C_3 \tag{59}$$

and

$$L_4=\frac{1}{\sin\theta_s\sin 2\theta_s}\,. \tag{60}$$

This expression is now completely general, *i.e.* no assumptions have been made concerning the size of the collimation parameters. Thus the Lorentz factor for the integrated polycrystalline intensity is $1/\sin\theta_s\sin 2\theta_s$, as anticipated in equation (4), independent of the instrumental resolution.

In the case where the detector collimation is relaxed, *i.e.* the assumption of equation (53), there is a very simple relation between the integrated intensity and the peak intensity, namely

$$\frac{\mathscr{I}_4}{I_4(\Delta q_x=0)}=(2\pi)^{1/2}\alpha_2\,. \tag{61}$$

We can also make an absolute comparison between the single-crystal intensity and the polycrystal intensity from the above expressions. For example, the ratio of the integrated intensities for a given reflection when α_2 and β_2 are large and the samples are the same size is simply

$$\frac{\mathscr{I}_4}{\mathscr{I}_3'}=\frac{m_B\alpha_2\beta_2}{4\sin\theta_s}\,. \tag{62}$$

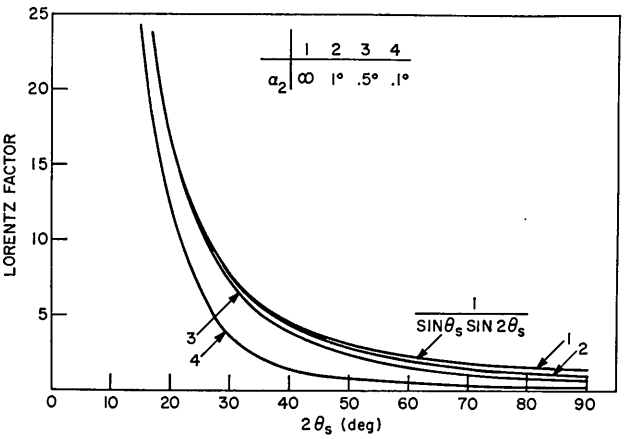

Fig. 7. The Lorentz factor L_4^0 as a function of $2\theta_s$ for four values of α_2.

Discussion

An interesting comparison can be made between the ratios of the peak intensities of a diffuse peak to a Bragg peak in a polycrystal and in a single crystal. This ratio in a single crystal is given by (I_1/I_3) at $\Delta\mathbf{q}=0$ and in a polycrystal by (I_2/I_4) at $\Delta q_x=0$. These ratios can be taken exactly using equations (21), (33), (41), and (51). However we will assume that the detector accepts all of the Bragg scattered intensity and that the extent of the resolution function is small compared with the diffuse peak. This assumption can be very nearly true in an experimental situation and is generally close enough to true to give us the relation for which we are looking. With this assumption then a comparison of the two ratios is written as

$$\left(\frac{\text{diffuse peak}}{\text{Bragg peak}}\right)_{\text{single}} \Big/ \left(\frac{\text{diffuse peak}}{\text{Bragg peak}}\right)_{\text{poly}} = \frac{(I_1'/I_3')_{\Delta q=0}}{(I_2'/I_4')_{\Delta q_x=0}} = \frac{m_B}{m_D}\left(\frac{K_0}{D}\right)^2 \frac{\beta_2}{2\sin\theta_s}$$

$$\times \left[\eta_{sh}^2 + \left(\frac{\tan\theta_s}{\tan\theta_M} - 1\right)^2 \alpha_1^2 + \frac{\tan^2\theta_B}{\tan^2\theta_M}\eta_M^2\right]^{1/2} \quad (63)$$

where $2\theta_s$ is the scattering angle for the Bragg peak.

We have made the additional assumption that the diffuse peak is isotropic about some point in reciprocal space. The order of magnitude of this ratio can be seen using typical values of $\beta_2 \simeq \frac{1}{2}^0$, $\sin\theta_s \simeq \frac{1}{2}^0$, $K_0 \simeq 2\pi/a_0$, the term in brackets in equation (63) $\simeq \frac{1}{2}^0$, and a value of $D \simeq 0{\cdot}1(2\pi/a_0)$ which is appropriate for the Cu–Mn alloy to be discussed later. Then the ratio is of the order of 0·01. *This means that the ratio of the peak intensities of a diffuse peak to a Bragg peak in a single crystal is of the order of 100 times smaller than the same ratio in a polycrystal.* Although this ratio is very sensitive to the particular values of the resolution parameters and also to the width of the diffuse scattering, the general conclusion can be made for most situations that in an experiment on a polycrystal the diffuse peaks are very prominent in comparison with the Bragg peaks, whereas in a single-crystal experiment these same diffuse peaks are very weak in comparison with the Bragg peaks. Another way of looking at this is to examine the ratios of the peak intensities in a polycrystal and a single crystal for both Bragg and diffuse peaks. In other words the ratios (I_2/I_1) and (I_4/I_3).

With the same assumptions we have

$$\frac{(\text{Bragg peak})_{\text{poly}}}{(\text{Bragg peak})_{\text{single}}} = \frac{I_4'(\Delta q_x=0)}{I_3'(\Delta q=0)} = \frac{m_B\beta_2\eta}{4\sin\theta_s} \simeq 10^{-4} \quad (64)$$

where η is the term in brackets in equation (63), and

$$\frac{(\text{diffuse peak})_{\text{poly}}}{(\text{diffuse peak})_{\text{single}}} = \frac{I_2'(\Delta q_x=0)}{I_1'(\Delta q=0)} = \frac{m_D D^2}{2K_0^2} \simeq 10^{-2}. \quad (65)$$

This expression shows that the relative intensity observed for a diffuse peak in a polycrystal to a diffuse peak in a single crystal depends mainly on the extent of the diffuse peak.

Example

As an example of the application of the above results, we shall discuss a study made on both single and polycrystalline samples of Cu-rich Cu–Mn alloys which exhibit short-range atomic ordering (Sato, Werner & Yessik, 1972). In particular we shall discuss here the results for well annealed samples of 25 at.% Mn. The measurements on both poly- and single-crystal samples were made on the same spectrometer under identical resolution conditions. The experimental values of the parameters involved are given in Table 1.

The results of a polycrystalline scan show a broad diffuse peak at a position corresponding to $\{\frac{1}{2}10\}$, similar to that first reported by Meneghetti & Sidhu (1957). The position of this peak is consistent with a short-range ordering of the $M=1$ type long-period superstructure (Sato & Toth, 1965). The results of a single-crystal scan along the $[h10]$ direction are shown in Fig. 8 and it can be seen that diffuse peaks occur at the positions $\frac{n}{2}10$ where n is an odd integer. Since these peaks all have the same scattering amplitude, the decrease of intensity from $\frac{1}{2}10$ to $\frac{7}{2}10$ is due to: (1) the Lorentz factor, (2) the temperature factor, and (3) a possible magnetic contribution from the short-range ordering of the moments on the Mn atoms. The shape of the diffuse peak was determined by a series of scans through the peak centered at $\frac{1}{2}10$ and is shown in Fig. 9. This measured shape was approximated by an ellipsoid and the Lorentz factor for the peak intensities was calculated directly from equation (30). This Lorentz factor is shown in Fig. 10 normalized to the value at the $\frac{7}{2}10$ position. The temperature factor was estimated as a weighted average of the pure Cu and pure Mn Debye model values, and the combined Lorentz and temperature factors are also shown in Fig. 10 normalized to the value at the $\frac{7}{2}10$ position. It can be seen

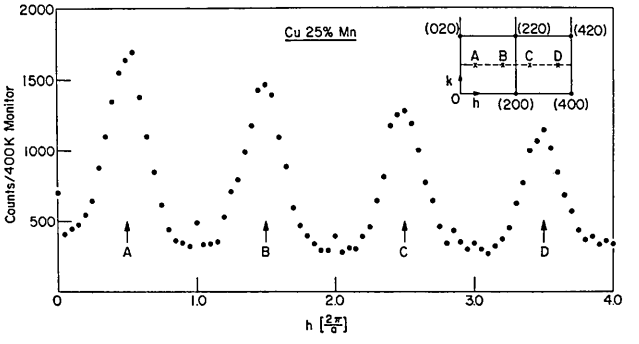

Fig. 8. Neutron intensity along the line $[h10]$ for a single crystal of Cu–25 at. % Mn.

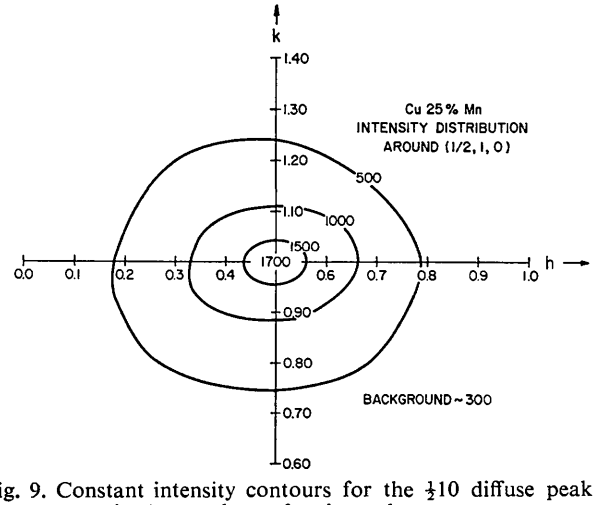

Fig. 9. Constant intensity contours for the $\frac{1}{2}10$ diffuse peak in the xy plane of reciprocal space.

that these two factors alone do not account for the entire intensity change. Therefore, it appears that there is a magnetic contribution to the diffuse peaks whose magnitude, estimated from the plots of Fig. 10, is approximately 20% of the nuclear scattering at the $\frac{1}{2}10$ position. Owing to the strong angular dependence of the magnetic scattering, it can be safely assumed that the intensity at $\frac{7}{2}10$ is essentially all nuclear.

A similar conclusion about the magnitude of the magnetic contribution has been made in a recent study on these alloys by Wells & Smith (1971). However, they did not take into account the angular dependence of the resolution correction (which in our case was about 5% in going from $\frac{1}{2}10$ to $\frac{7}{2}10$, and therefore the precise nature of the magnetic correlations remains unknown.

In addition, it was found desirable to make a direct comparison of the single and polycrystalline peaks in order to ensure that all of the diffuse scattering seen in the polycrystalline scan actually corresponds to the $\frac{1}{2}10$ single-crystal peak. This comparison was made by normalization to a Bragg peak. The Bragg peak considered was the 200 peak for which $m_B=6$ and $\theta_s=16{\cdot}85°$, and the peak intensities were calculated using equations (48) and (52). The $\frac{1}{2}10$ diffuse peak for which $m_D=24$ was considered to be ellipsoidal with characteristic widths $D_{x'}=0.14$, $D_{y'}=0.095$, and $D_{z'}=0.095$ in units of $2\pi/a_0$. The peak intensities were calculated using equation (21) for the single crystal and the expression for an ellipsoidal diffuse peak in a polycrystal (not shown here explicitly). The expected ratio thus calculated of normalized single-crystal diffuse peak to normalized polycrystal diffuse peak is given by

$$\frac{(I_1/I_3)\Delta q=0}{(I_2/I_4)\Delta q_x=0)}=2{\cdot}23\times10^{-3}. \qquad (66)$$

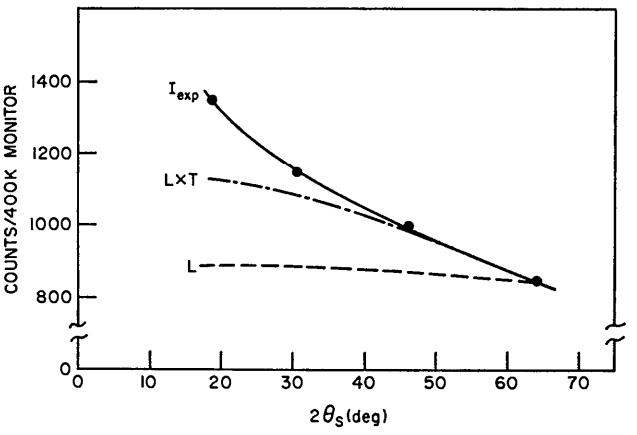

Fig. 10. The contributions of the Lorentz factor, temperature factor, and magnetic form factor to the decrease in intensity of the peaks of the diffuse scattering along the line [h10]. The experimental intensities are denoted by I_{exp}, the Lorentz factor by L, and the combined Lorentz and temperature factors by $L\times T$. The difference between the curves I_{exp} and $L\times T$ is attributed to magnetic scattering.

The actual experimental values obtained for a 400K monitor count are as follows:

$$I(\tfrac{1}{2}10)_{single}=1350 \quad I(200)_{single}=1{\cdot}98\times10^6 \qquad (67)$$
$$I(\tfrac{1}{2}10)_{poly}=360 \quad I(200)_{poly}=1550$$

and thus the experimental ratio is $2{\cdot}94\times10^{-3}$. This agreement is considered quite good, especially since no correction has been made for extinction in the single-crystal Bragg peak and confirms that all of the polycrystalline diffuse peak is accounted for by the $\frac{1}{2}10$ single-crystal peak. It also confirms the analytical result that a diffuse peak is much smaller relative to a Bragg peak in a single crystal than in a polycrystal.

APPENDIX *A*

Coefficients of the resolution function for relaxed in-pile collimation

The coefficient R_0 is given by

$$R_0=\frac{\pi P_0P_1P_2}{b^2k_I^2\sqrt{AA'}}. \qquad (A1)$$

This expression differs from that given by Cooper & Nathans [equation (19), 1968*b*] by a factor $1/b^2k_I^2$ since the form of the scattering cross section used by them differs from the one used here.

The elements of the matrix M_{kl} are given by

$$\begin{aligned}M_{11}&=s_1^2-s_0^2s_1^2/A'\\ M_{12}&=s_1s_2-(s_0s_1)\,(s_0s_2+p_0p_2)/A'\\ M_{22}&=s_2^2+p_2^2-(s_0s_2+p_0p_2)^2/A'\\ M_{33}&=1/(k_1^2\beta_1^2+k_1^2\beta_2^2)\end{aligned} \qquad (A2)$$

where

$$\begin{aligned}s_0&=\left(1-\frac{a}{b}\tan\theta_M\right)\Big/k_I\eta_M \quad r_0=\frac{1}{k_I\alpha_1}\\ s_1&=-\left(\frac{1}{2b}\right)\tan\theta_M/k_I\eta_M \quad p_0=\frac{1}{k_I\alpha_2}\\ s_2&=\frac{a}{2b^2}\tan\theta_M/k_I\eta_M \quad p_2=-\frac{1}{b}\,\frac{1}{k_I\alpha_2}\end{aligned} \qquad (A3)$$

and

$$\begin{aligned}A'&=s_0^2+r_0^2+p_0^2\\ A&=1/k_1^2\beta_1^2+1/k_I^2\beta_2^2.\end{aligned} \qquad (A4)$$

Since the vertical resolution is assumed to be independent of the horizontal resolution then

$$M_{k3}=M_{3l}=0 \quad \text{for } k,l\neq3.$$

The definitions of the parameters involved in these equations are given in Table 1.

In order to perform an experiment on a Cu–25 at.% Mn sample, to be described more fully later, particular values of the instrumental parameters were chosen. The parameters η_M and α_1 were obtained from a series of rocking curves on a perfect Si crystal. The param-

eter β_1 was obtained by measuring the intensity as a function of tilt angle in the parallel position. The collimation parameters for the detector, α_2 and β_2, were obtained from the collimator geometry. The parameter η_{sh} was obtained from a rocking curve of the sample crystal in the parallel position, and η_{sv} was assumed equal to η_{sh}. The values of these parameters are shown in Table 1.

APPENDIX *B*

Coefficients of the intensity equation for diffuse scattering from a mosaic single crystal

The coefficient C_0 is given by

$$C_0=(2\pi)^{3/2}R_0'\left(N_{33}'+\frac{1}{D_{z'}^2}\right)^{-1/2}\left(N_{22}'+\frac{1}{D_{y'}^2}\right)^{-1/2}\times\left(N_{11}'-\frac{N_{12}'^2}{N_{22}'+\frac{1}{D_{y'}^2}}+\frac{1}{D_{x'}^2}\right)^{-1/2} \quad (B1)$$

and the matrix C_{kl} is given by

$$C_{11}=\frac{1}{D_{x'}^2}-\frac{1}{D_{x'}^4}\frac{1}{\left(\frac{1}{D_{x'}^2}+N_{11}'-\frac{N_{12}'^2}{N_{22}'+\frac{1}{D_{y'}^2}}\right)}$$

$$C_{12}=\frac{1}{D_{x'}^2}\frac{1}{D_{y'}^2}\frac{\left(\frac{N_{12}'}{N_{22}'+\frac{1}{D_{y'}^2}}\right)}{\left(\frac{1}{D_{x'}^2}+N_{11}'-\frac{N_{12}'}{N_{22}'+\frac{1}{D_{y'}^2}}\right)} \quad (B2)$$

$$C_{22}=\frac{1}{D_{y'}^2}-\frac{1}{D_{y'}^4}\frac{1}{\left(N_{22}'+\frac{1}{D_{y'}^2}\right)}\times\left[1+\frac{N_{12}'^2}{\left(N_{22}'+\frac{1}{D_{y'}^2}\right)\left(\frac{1}{D_{x'}^2}+N_{11}'-\frac{N_{12}'^2}{\left(N_{22}'+\frac{1}{D_{y'}^2}\right)}\right)}\right]$$

$$C_{33}=\frac{1}{D_{z'}^2}\frac{N_{33}'}{\left(N_{33}'+\frac{1}{D_{z'}^2}\right)}.$$

The N_{kl} are the transformed M_{kl} values, *i.e.*

$$\mathsf{N}'=\mathsf{T}\mathsf{M}'\mathsf{T}^{-1} \quad (B3)$$

where T is the transformation matrix.

References

COOPER, M. J. & NATHANS, R. (1968*a*). *Acta Cryst.* A**24**, 481–484.

COOPER, M. J. & NATHANS, R. (1968*b*). *Acta Cryst.* A**24**, 619–624.

International Tables for X-Ray Crystallography (1959). Vol. II, p. 266. Birmingham: Kynoch Press.

MENEGHETTI, D. & SIDHU, S. S. (1957). *Phys. Rev.* **105**, 130–135.

SATO, H. & TOTH, R. S. (1965). *Alloying Behavior in Concentrated Solid Solutions*, pp. 295–419. Edited by T. B. MASSALSKI. New York: Gordon and Breach.

SATO, H., WERNER, S. A. & YESSIK, M. (1972). Conference on Magnetism and Magnetic Materials 1971, *AIP Conf. Proc. No.* 5, pp. 508–512.

WELLS, P. & SMITH, J. H. (1971). *J. Phys. F*, **1**, 763–770.

Acta Cryst. (1973). A**29**, 382

The Solution of Non-Centrosymmetric Crystal Structures by Symbolic Tangent Refinement

BY COLIN T. GRAINGER

School of Physics, The University of New South Wales, Kensington, N.S.W. 2033, *Australia*

(*Received* 18 *December* 1972; *accepted* 24 *January* 1973)

Starting from a restricted set of numerical and symbolic phase angles, the tangent formula is applied iteratively to determine numerical and symbolic phase indications for the other reflexions. Numerical values are then systematically substituted for the symbols to determine which combinations are most likely to yield the solution.

Introduction

While for centrosymmetric structures automatic computer programs using symbolic methods have been widely successful (Germain & Woolfson, 1968; Ahmed, 1970; Bednowitz, 1970; Dewar, 1970; Stewart, 1970), the symbolic approach for non-centrosymmetric structures has usually been restricted to use of the sum-of-angles formula in the early stages to determine likely numerical values of the symbols, after which further phasing is completed by numerical tangent refinement (Karle & Karle, 1966; Schenk, 1971; Dewar, 1970). Ideally this process leads to a single solution.

The program *SYMTAN* described here differs from